Advancing Hydrogen Storage in Aviation: Stress State of Discretely Loaded All-Composite Double-Walled Vacuum-Insulated Cryo-Compressed Vessels

Poorte, V.K.; Bergsma, O.K.; van Campen, J.M.J.F.; Alderliesten, R.C.

DOI
10.2514/6.2025-0621

Publication date
2025

Document Version
Final published version

Published in
Proceedings of the AIAA SCITECH 2025 Forum

AIAA SciTech Forum
6-10 January 2025, Orlando, FL
AIAA SCITECH 2025 Forum

10.2514/6.2025-0621

Advancing Hydrogen Storage in Aviation: Stress State of Discretely Loaded All-Composite Double-Walled Vacuum-Insulated Cryo-Compressed Vessels

Victor K. Poorte*, Otto K. Bergsma, Julien M.J.F. van Campen, and Renè C. Alderliesten
Faculty of Aerospace Engineering, Delft University of Technology, 2629 HS Delft, The Netherlands

Hydrogen is a promising candidate for achieving aviation sustainability, but storage aboard aircraft presents significant challenges. All-composite, double-walled, vacuum-insulated cryo-compressed storage vessels offer a potential solution by achieving high volumetric and gravimetric efficiencies. Load transfer connections between the tank's shells and the surrounding structure introduce concentrated loads in the composite shells. This work develops analytical models to characterize the stress state in composite shells under discrete in-plane loading, showing how stress concentrations decay and how laminate selection influences the decay rate. Discrepancies between the analytical and numerical models are noted, with suggestions for improving both. Additionally, the current model's limitations due to the number of roots obtained from the governing equations are addressed by proposing additional boundary conditions. This research supports the structural and thermal analysis of composite hydrogen storage vessels, aiding the adoption of hydrogen as a sustainable aviation fuel.

Nomenclature

Greek symbols

α	=	Angle between loading points
ω	=	Load introduction angle
Φ	=	Airy stress function
ϕ	=	Roots of the differential equation, with i for in-plane and o for out-of-plane
σ_x	=	In-plane stress in the axial direction
σ_θ	=	In-plane stress in the hoop direction
$\tau_{x\theta}$	=	Shear stress in the axial-circumferential plane
θ	=	Coordinate in the circumferential direction

Latin symbols

a_{ij}	=	Compliance matrix entries
$C_{i,k}$	=	In-plane scaling factors
$C_{o,k}$	=	Out-of-plane scaling factors
D_{ij}	=	Flexural matrix entries
$f_n(x)$	=	In-plane stress function
$g_n(x)$	=	Out-of-plane displacement function
H	=	Thickness of the tank/laminate
L	=	Length of the tank, half the length is used for symmetry
m	=	Number of loading points
N_x	=	In-plane axial load
N_θ	=	In-plane hoop load
$N_{x\theta}$	=	In-plane shear load
R	=	Radius of the tank
$w(x,\theta)$	=	Out-of-plane displacement
x	=	Coordinate in the axial direction

*Contact: V.K.Poorte@tudelft.nl.

I. Introduction

Aviation has several options to meet its sustainability goals, including sustainable aviation fuel and battery-electric technologies. This paper focuses on hydrogen and one of its primary challenges: storage. With a gravimetric energy density of 120 MJ/kg, hydrogen is a highly suitable energy carrier by mass. However, with an assumed density of 70 kg/m^3, its volumetric energy density is approximately four times lower than that of traditional aviation fuel. To achieve this density, hydrogen must be cooled to cryogenic temperatures and pressurized. Consequently, it must be stored in an insulated, pressurized vessel that meets aviation requirements for both gravimetric and volumetric efficiency.

An all-composite vacuum-insulated storage vessel offers a potential solution, as depicted in Figure 1. Such a vessel could be integrated into the aircraft's primary structure, enhancing airframe integration and reducing overall aircraft mass. However, this integration requires the vessel to withstand additional loads beyond thermal and pressure-induced stresses. These loads may arise from dynamic fuel movements, thermal expansion mismatches between components, or external forces introduced into the tank.

This study focuses on the structural analysis of composite cylinders, representing the body section of the fuel tank shown in Figure 1, as these components are envisioned to bear additional loads.

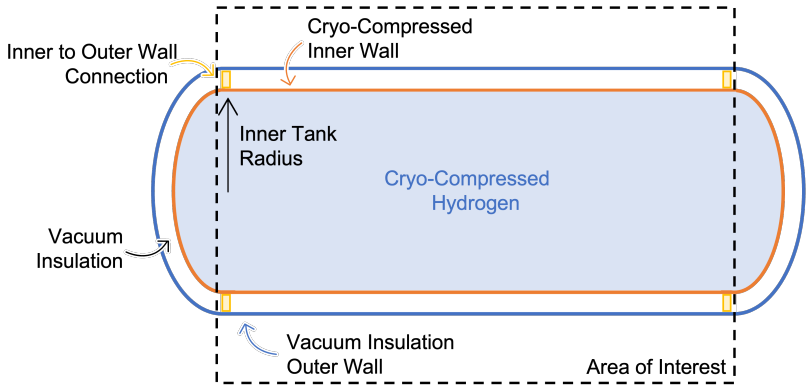

Fig. 1 Example of a double-walled vacuum insulated storage vessel.

The current work builds upon prior research by the authors [1, 2], which investigates integrating all-composite, double-walled, vacuum-insulated hydrogen storage vessels into an aircraft's primary structure. Previous studies introduced methods to analyze pressurized, axially loaded, and thermally loaded composite cylinders. However, [1] assumes a continuous load introduction at the cylinder edges, whereas actual axial loads are likely to be introduced at discrete points, as illustrated in Figure 2. While [2] addresses this limitation, the coupling between in-plane and out-of-plane behavior of the vessel remains absent. This paper aims to incorporate this coupling.

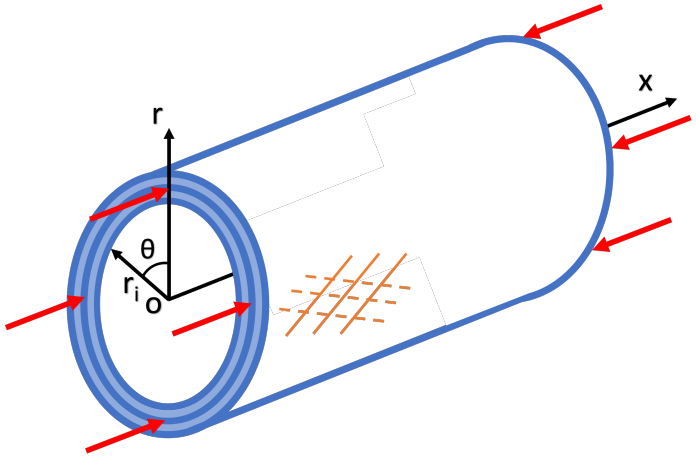

Fig. 2 Coordinate system and loading of multi-loaded composite cylinder.

Discrete loading points are a critical design consideration. A continuous load introduction skirt would result in excessive thermal bridging between the tank's shells and the surrounding structure, negatively impacting tank thermal efficiency. During preliminary design, engineers must balance thermal and structural requirements. Thermal considerations typically favor minimizing the size and number of contact points, while structural considerations often favor the opposite. Simple and efficient models can help identify this balance point during early design stages.

This study builds on prior work by the authors, which examined the thermal performance of hydrogen storage vessels. Future efforts will focus on coupling thermal and structural models to optimize the balance between thermal and structural requirements.

This work contributes to developing methods for evaluating the viability of hydrogen storage vessels as primary structural components in aviation applications. The proposed methods are designed for straightforward implementation, facilitating preliminary design processes. Ultimately, this research supports the development of hydrogen-powered aircraft, advancing the energy transition within the aviation industry.

II. Methods

A. Closed Form Solution

The method for determining the stress state in a discretely loaded cylinder is based on the work of C. Kassapoglou and G. Bauer [3], which originally analyzed a discretely loaded plate. As such, the current work also assumes the cylinder to be homogenous and orthotopic and have a symmetric laminate, resulting in a null coupling matrix, and only includes linear strains. The cited work was further developed by the current authors to enable the analysis of periodically loaded cylinder [2]; the mentioned work does not account for in-plane and out-of-plane coupling, present in cylinders, which the current work aims to include. Consequently, the compatibility equation must be modified to incorporate out-of-plane behavior, as shown in Equation 1. The Airy stress function (Φ) is used in the equation to facilitate subsequent derivations. The a terms represent the entries of the compliance matrix, computed using classical laminate theory. Here, $w(x,\theta)$ denotes the out-of-plane displacement, while R is the radius of the tank, and x and θ correspond to the coordinate system depicted in Figure 2.

$$a_{22}\left(\frac{\partial^4}{\partial x^4}\Phi(x,\theta)\right) + (2a_{12}+a_{66})\left(\frac{\partial^4}{\partial\theta^2\partial x^2}\Phi(x,\theta)\right) + a_{1I}\left(\frac{\partial^4}{\partial\theta^4}\Phi(x,\theta)\right) = -\frac{\frac{\partial^2}{\partial x^2}w(x,\theta)}{R} \tag{1}$$

For convenience, the relations between the Airy stress function and the in-plane loads are summarized in Equation 2. These are then used to compute the stresses by dividing them by the laminate thickness H.

$$N_x = \frac{\partial^2\Phi}{\partial\theta^2} \quad N_\theta = \frac{\partial^2\Phi}{\partial x^2} \quad N_{x\theta} = -\frac{\partial^2\Phi}{\partial x\partial\theta} \tag{2}$$

As there are two unknowns—namely, the Airy stress function and the out-of-plane displacement— an additional equation is required. The out-of-plane equilibrium equation, as depicted in Equation 3, is used. Here, the D terms represent the entries of the flexural matrix, also calculated using classical laminate theory.

$$\mathrm{D}_{11}\left(\frac{\partial^4}{\partial x^4}w(x,\theta)\right) + (2\mathrm{D}_{I2}+4\mathrm{D}_{66})\left(\frac{\partial^4}{\partial\theta^2\partial x^2}w(x,\theta)\right) + \mathrm{D}_{22}\left(\frac{\partial^4}{\partial\theta^4}w(x,\theta)\right) = \frac{\frac{\partial^2}{\partial x^2}\Phi(x,\theta)}{R} \tag{3}$$

These equations are solved while respecting the boundary conditions presented below. In the boundary conditions, m represents the number of loading points, ω is the load introduction angle (indicating the section over which the load acts), α is the angle between loading points (computed as $2\pi/m$), H is the tank thickness, and L is the tank length (which can be taken as half the total length due to assumed symmetry).

$$\begin{aligned} \sigma_x(x=0) &= \frac{F}{mR\omega H} \quad \text{for} \quad i\alpha - \frac{\omega}{2} \le \theta \le i\alpha + \frac{\omega}{2} \quad \text{for} \quad i = 0\ldots m-1 \\ \sigma_x(x=0) &= 0 \quad \text{for} \quad i\alpha + \frac{\omega}{2} \le \theta \le (i+1)\alpha - \frac{\omega}{2} \quad \text{for} \quad i = 0\ldots m-1 \end{aligned} \tag{4}$$

$$\sigma_x(x=L) = \frac{F}{2\pi RH} \tag{5}$$

$$\tau_{x\theta}(x = 0) = 0 \tag{6}$$

$$\tau_{x\theta}(\theta = i\frac{\alpha}{2}) = 0 \quad \text{for} \quad i = 1...m \tag{7}$$

$$\frac{\partial w}{\partial x}(x = L) = 0 \tag{8}$$

$$\frac{\partial w}{\partial \theta}(\theta = i\frac{\alpha}{2}) = 0 \quad \text{for} \quad i = 1...m \tag{9}$$

A visual representation of the boundary conditions is shown in Figure 3, which illustrates a single load section defined by the angle α. The figure also includes the load introduction angle, ω. For simplicity, a square is used to represent a section of the cylinder, serving as an illustrative approximation. In fact α and ω may seem line lengths, though these are angles in the actual coordinate system. Dashed edges indicate the boundaries where symmetries are applied: the horizontal edges reflect rotational symmetry, while the vertical edge represents lengthwise symmetry.

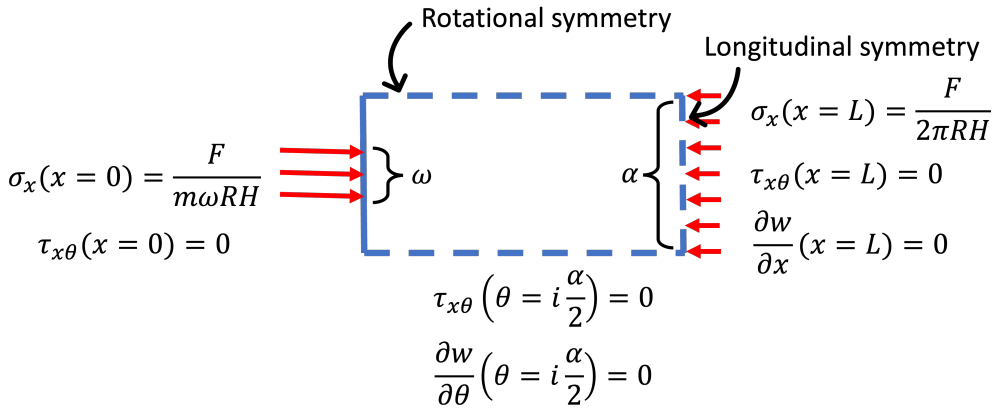

Fig. 3 Free body diagram of a single load section, denoting boundary stresses and rotations.

Based on these boundary conditions, assumptions are made for the Airy stress function and displacement function, as given in Equation 10 and Equation 11, respectively. The functions are chosen such that the trigonometric terms satisfy the boundary conditions at a given angle θ. Boundary conditions for x values are later used to define the $f_n(x)$ and $g_n(x)$ functions. It should be clear that $f_n(x)$ and $g_n(x)$ differ per n values, explaining the subscript.

$$\Phi(x, \theta) = \sum_n f_n(x) \cos\left(\frac{n\pi\theta}{\alpha}\right) \tag{10}$$

$$w(x, \theta) = \sum_n g_n(x) \cos\left(\frac{n\pi\theta}{\alpha}\right) \tag{11}$$

The assumed functions are plugged into the equilibrium equation and compatibility equations. The common trigonometric terms can be dropped, resulting in a system of two differential equations for the two functions, as presented in equations 12 and 13.

$$a_{22}\frac{\mathrm{d}^4 f_n(x)}{\mathrm{d}x^4} - 2\frac{\mathrm{d}^2 f_n(x)}{\mathrm{d}x^2}\left(\frac{n\pi}{\alpha}\right)^2 a_{12} - \frac{\mathrm{d}^2 f_n(x)}{\mathrm{d}x^2}\left(\frac{n\pi}{\alpha}\right)^2 a_{66} + a_{11} f_n(x)\left(\frac{n\pi}{\alpha}\right)^4 = -\frac{\frac{\mathrm{d}^2 g_n(x)}{\mathrm{d}x^2}}{R} \tag{12}$$

$$\mathrm{D}_{11}\frac{\mathrm{d}^4 g_n(x)}{\mathrm{d}x^4} - 2\frac{\mathrm{d}^2 g_n(x)}{\mathrm{d}x^2}\left(\frac{n\pi}{\alpha}\right)^2 \mathrm{D}_{12} - 4\frac{\mathrm{d}^2 g_n(x)}{\mathrm{d}x^2}\left(\frac{n\pi}{\alpha}\right)^2 \mathrm{D}_{66} + \mathrm{D}_{22} g_n(x)\left(\frac{n\pi}{\alpha}\right)^4 = \frac{\frac{\mathrm{d}^2 f_n(x)}{\mathrm{d}x^2}}{R} \tag{13}$$

The system is first solved for $g(x)$. This is done by rearranging Equation 13, to obtain a function for $\frac{\mathrm{d}^2 f(x)}{\mathrm{d}x^2}$, which is then used to substitute into the derivatives of equation 12, resulting in an eighth-degree differential equation, which can be solved by finding the eight roots of the polynomial. Consequently, the solution for $g(x)$ becomes a sum of exponentials as depicted in Equation 14, where ϕ_o are the roots of the polynomial. Note that the roots differ for each n term. Finally, $C_{o,k}$ are the out-of-plane scaling factors, later determined using the boundary conditions.

$$g_(x) = \sum_{k=0}^{7} C_{o,k} e^{\phi_{o,k} x} \tag{14}$$

The in-plane stress function $f_n(x)$ is determined using Equation 12 and is given by the sum of the homogeneous solution and the complementary solution. The homogenous solution is a sum of exponentials, as depicted in Equation 15, where $C_{i,k}$ are the in-plane scaling factors, later determined using the boundary conditions, and ϕ_i are the in plane roots of the fourth order homogeneous differential equation. The particular solution is determined using the method of undetermined coefficients and the previously derived $g_n(x)$

$$f(x) = \sum_{k=0}^{3} C_{i,k} e^{\phi_{i,k} x} \tag{15}$$

There are twelve unknown coefficients: four for in-plane stress and eight for out-of-plane displacement, with only four boundary conditions available. Therefore, the nature of the roots must be analyzed. For in-plane roots, there are two pairs of solutions, each consisting of one positive and one negative root, or a single pair in the case of repeated roots. Complex roots appear as conjugate pairs. Out-of-plane roots can be real, complex, or a combination of both. The root types depend on the summation index n, so multiple solution sets may exist for a single tank.

As suggested in [3], only the negative roots are considered. This ensures that both the stresses and the displacements converge to a far-field value, preventing them from growing unbounded. A subsequent step involves separating the complex solutions into exponential and oscillatory parts. The oscillatory part is neglected, as it is assumed to be negligible compared to the exponential part.

At this point, the four in-plane coefficients are reduced to two. The number of out-of-plane coefficients depends on the nature of the roots: if all the roots are complex, only two coefficients remain; if the roots are a mixture of complex and real, three coefficients remain; and if the roots are all real, four coefficients remain. Given the current set of boundary conditions, the system can only be fully determined when all the out-of-plane roots are complex. This is further discussed in subsection III.B.

The boundary condition defined in Equation 4 needs to be modified to account for the discontinuous load in a single equation. Similar to [3], an integral is taken over the loading edge along the circumference of the vessel. Both sides of the equation are multiplied by a $\cos\left(\frac{q\pi\theta}{\alpha}\right)$ factor, to avoid the integral of cos over its domain becoming null, as depicted in Equation 16.

$$\int_0^{2\pi} \sigma_x(x=0) \cos\frac{q\pi\theta}{\alpha} d\theta = \int_0^{2\pi} \left(-\sum f_n(x=0) \left(\frac{n\pi}{\alpha}\right)^2 \cos\frac{n\pi\theta}{\alpha} \right) \cos\left(\frac{q\pi\theta}{\alpha}\right) \mathrm{d}\theta \tag{16}$$

Implementing the periodic discrete stresses on the right-hand side and trigonometric relations on the right-hand side, the boundary condition becomes as depicted in Equation 17.

$$\frac{2F}{m\omega RH} \left(\frac{n\pi}{\alpha}\right)^{-1} \sin\left(\frac{n\pi\omega}{2\alpha}\right) \sum_{i=0}^{m-1} \cos(i\pi) = -f_n(x=0)\pi \left(\frac{n\pi}{\alpha}\right)^2 \tag{17}$$

B. Numerical Model

A numerical model is developed in Abaqus to verify the results obtained from the closed-form solution. This model employs a shell-type approximation, utilizing S4R elements with a mesh size of 1 mm. The element length is chosen to be sufficiently small to accurately capture the decay of the concentrated load, as discussed by Kassapoglou [3]. To reduce computational effort, the model takes advantage of rotational symmetry by considering only a single loading point. Additionally, lengthwise symmetry along the x-axis of the tank is assumed, such that only one side of the tank is modeled. The concentrated load is applied directly to the nodes of the mesh.

C. Case Study Properties

A case study is conducted to verify the analytical model. To do so, values for the vessel, laminate, and loading are required. The dimensions of the tank are provided in Table 1. Note that the length refers only to the analyzed section of the tank, representing half the total length of the structure. The material properties are listed in Table 2. A laminate is created from the provided laminae with the following layup: $[\pm 45/0/\pm 45]$. The loading conditions for the vessel are detailed in Table 3.

Table 1 Tank dimensions.

Property	Symbol	Value	Unit
Radius	R	0.5	m
Length	L	1.0	m
Laminate thickness	H	0.5715	mm

Table 2 Lamina properties.

Property	Symbol	Value	Unit
Longitudinal modulus	E_{11}	73.1	GPa
Traverse modulus	E_{22}	73.1	GPa
Shear modulus	G_{12}	5.17	GPa
Poisson ratio	ν_{12}	0.05	-
Ply thickness	t	0.1905	mm

Table 3 Loading conditions.

Property	Symbol	Value	Unit
Total axial load	F	25.0	kN
Number of loading points	m	6	-
Load introduction angle	ω	$\pi/12$	rad

III. Results

A. Analytical Model Verification

Figure 4a shows the longitudinal stress (σ_x) at the loading edge. This chart is intended to replicate the boundary condition outlined in Equation 5. The figure demonstrates that the desired behavior is achieved. The blue line, representing the stress along the circumference of the vessel, focused on a single loading section, exhibits wave-like behavior characteristic of the Fourier series. Increasing the number of summation terms smooths this behavior, though limitations are discussed in subsection III.B.

In Figure 4b, the results from both the analytical and numerical models are presented. These plots show the longitudinal stress (σ_x) along the length of the cylinder at the center of a loading location for $\theta = 0$. Both models show the expected stress decay as the concentrated load is distributed along the vessel's circumference. On the left side of the figure, a discrepancy between the numerical and analytical models is evident. While the analytical model tends toward the expected value of 55.7 MPa, the numerical model's value does not exceed 30.0 MPa. Additionally, the numerical model exhibits unexpected wave-like behavior.

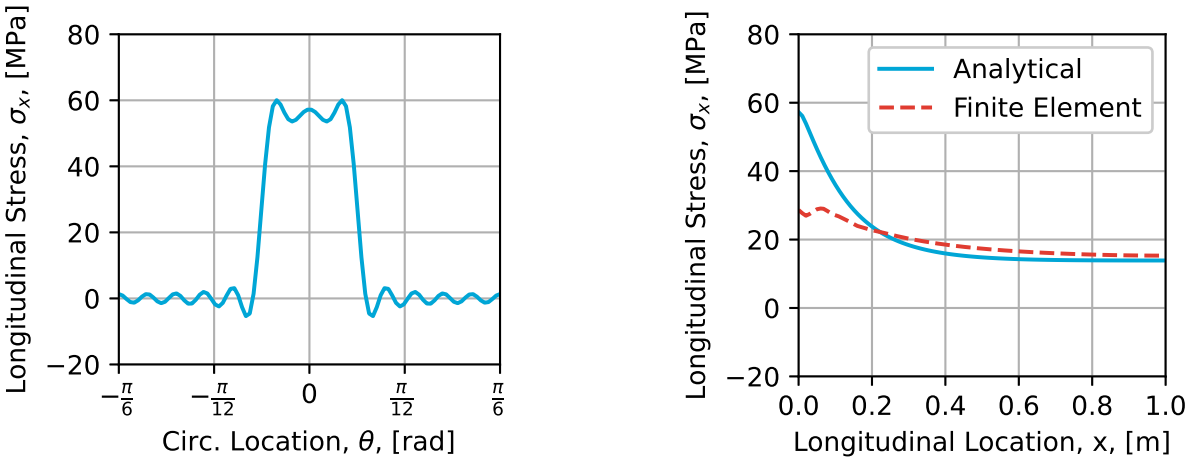

(a) **(b)**

Fig. 4 Stress development in the cylinder: (a) Longitudinal stress (σ_x) along the circumference of the vessel, at the loading edge (x=0), (b) longitudinal stress (σ_x) along the length of the tank at a loading location ($\theta = 0$).

The discrepancy between the numerical and analytical models may stem from multiple factors. One possibility is that the concentrated load in the numerical model is not aligned with the rotation of the nodes. As the shell rotates at the loading edge, the loading has both in-plane and out-of-plane components. This could explain the lower stress values reported in Figure 4b. This will be investigated further in future work. The wave-like behavior near the loading edge, indicated by the orange-dashed line in Figure 4b, cannot be explained by shell rotation alone. The cause of this behavior is still unclear, but it resembles patterns observed in transverse stress (σ_θ) near the loading edge [2, 3]. The authors suspect that this anomaly is related to the discrete loading. The discontinuous nature of the loading is likely contributing to the observed irregular behavior. In reality, the stress should increase gradually along the circumference from 0 to 55.7 MPa, not abruptly. To address this, future work will explore how modifying the shape of the load introduction affects this behavior and whether such anomalies can be resolved.

B. Roots Analysis

In subsection II.A, it is discussed that only complex roots are valid for the current model, as real and mixed roots do not provide enough boundary conditions to determine the scaling coefficients. In the current case study, 200 summation terms are used, though [3] suggests that 80 terms are sufficient for similar analyses. The choice of summation terms is based on the smoothness of the stress at the loading edge, as shown in Equation 5. Of the 200 summation terms, 27 terms have complex out-of-plane roots, one has all real roots, and the remaining 172 have mixed roots. Therefore, only the 27 terms with complex roots contribute to the solution, while the other 163 terms are neglected. The in-plane roots are all repeated roots. It is important to note that these results are specific to the current case study, and variations in loading conditions or tank properties will affect the root types.

Several approaches can be considered to increase the number of boundary conditions and thus include more root types. The first approach is to incorporate the rotation of the loading edge. This could be set to zero or equated with the rotation of the transition section between the tank body and the dome sections. However, a potential complication arises due to the interaction of the complex stress state at the transition, caused by laminate rotation [4] and the load introduction point. To address this, it is hypothesized that load introduction points should be placed further away from the transition area.

A second approach involves incorporating the out-of-plane work of the plate. However, two challenges arise: first, computing the work requires a product of stresses and out-of-plane displacements, making the problem nonlinear and complicating a closed-form solution. Second, for applications such as hydrogen storage, where pressure is required to achieve viable gravimetric and volumetric efficiencies, the out-of-plane work cannot be set to zero. As a result, this boundary condition cannot be applied.

Another possibility is to relate out-of-plane displacement to hoop strain in the far field. However, this boundary condition lacks sufficient detail to capture the localized effect of the discrete load at the loading edge. As the discrete load is applied at the edge, a boundary condition based on far-field behavior is suspected not to accurately represent this effect. These limitations and potential alternatives will be explored in future work.

Additionally, the current analytical model omits the θ displacement boundary condition at the edges where rotational symmetry is assumed between two loading points. The θ displacement at these edges should be zero, which would affect the transverse stress (σ_θ) and may help align the numerical and analytical models.

When incorporating the aforementioned boundary conditions, future studies will explore scenarios where the inclusion of real or mixed roots requires additional boundary conditions. Specifically, when five boundary conditions are applied, the system becomes overdetermined for complex out-of-plane roots. Similarly, when six boundary conditions are used to include all-real roots, the system also becomes overdetermined for mixed roots. In such cases, the behavior of the overdetermined system will be analyzed to understand how it affects the solution. Alternatively, a hierarchy in boundary conditions may need to be established, such that different boundary conditions are applied depending on the root type.

C. Model Potential

The potential implementation of the model is explored in this section. Closed-form solutions offer fast results, making them valuable for quick insights, particularly during the preliminary design phase of a hydrogen fuel tank. Numerical models, while more detailed, can be time-consuming to set up and run. In contrast, an analytical model provides immediate feedback, which is advantageous for exploring the effects of connection or loading points in composite hydrogen storage vessels, areas that are not yet fully understood.

One potential insight from the analytical model is the transverse and shear stress distribution along the circumference of the tank, at a specific location along its length. As depicted in Figure 5, the same test case from subsection II.C is used, with stress values obtained at $x = 5\,\text{cm}$. On the left side of the figure, the transverse stress (σ_θ) is shown, and on the right, the shear stress ($\tau_{x\theta}$). In comparison to both the flat plate model in the work of Kassapoglou and Bauer [3] and the cylindrical model derived by the current authors [2], the transverse stress does not decay to zero. Instead, it stabilizes at approximately 10 MPa. Similarly, the shear stress does not decay smoothly but gradually approaches zero to meet the rotational symmetry requirement. In previous work of the authors [3], it was taken into account that the transverse stress would not necessarily decay to zero, due to the interaction of two loading points, though in the current figure this is clearly not non-zero due to loading point interaction, due to the shape of the stress, which displays asymptotic behavior. This shows the necessity of including the vessel's out-of-plane behavior.

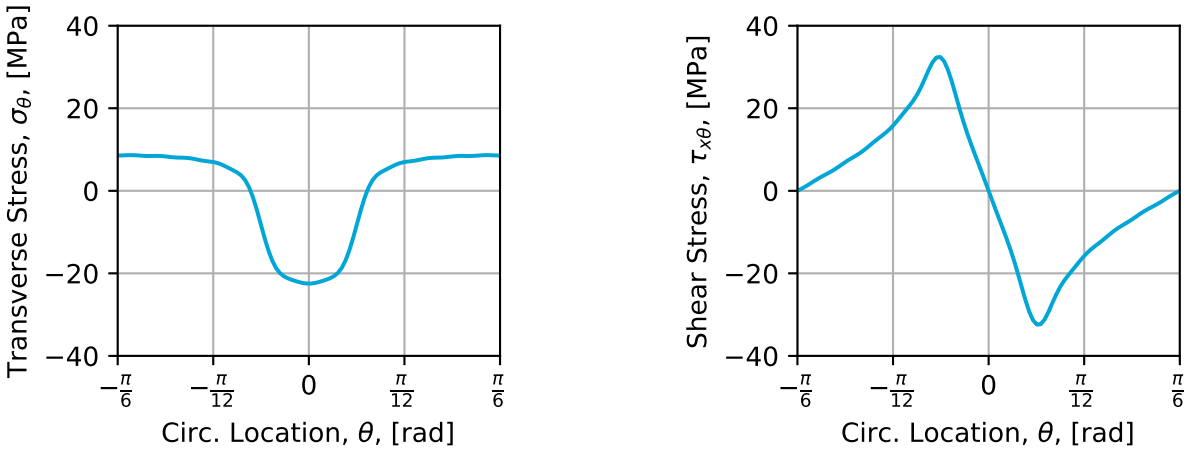

(a) **(b)**

Fig. 5 Stresses along the circumference of the pressure vessel at x=5 cm: (a) transverse stress (σ_θ) and (b) shear stress ($\tau_{x\theta}$).

A key aspect of the concentrated load is the rate at which the stress decays to far-field values. This is inherently captured by the exponentials and the roots of the differential equations, which are influenced by the laminate and tank properties. Figure 6 illustrates how the laminate affects the stress decay. Designers can choose whether a rapid or gradual stress decay is more desirable based on various design factors. As shown in Figure 6, the laminate's layup significantly influences the rate of decay, with the ±45 layers helping to distribute the loads more gradually. It is important to note that the initial stress values on the left-hand side of the chart differ, though these values should ideally be the same. The discrepancy is attributed to the sinusoidal behavior of the stress, as described when analyzing Figure 4a.

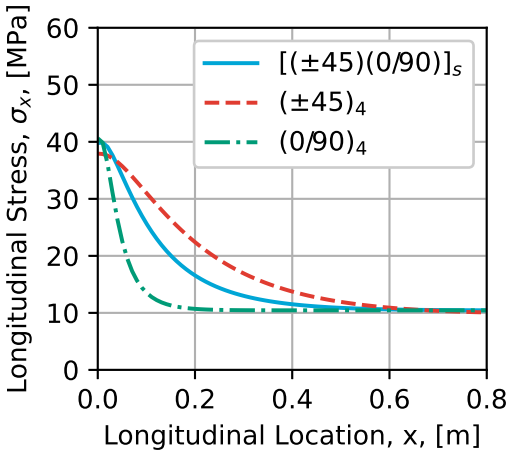

Fig. 6 Decay of the longitudinal stress (σ_x) along the length of the tank in the center line of a load introduction point ($\theta = 0$) for different layups.

IV. Conclusions and Recommendations

In this work, a closed-form solution is presented for analyzing the stress state of a composite cylinder subjected to periodic discrete in-plane loads at its free edge. This is particularly relevant for hydrogen storage vessels, where composite materials are increasingly used to meet the demands of lightweight, high-strength designs. The model provides insights that can guide the design of hydrogen storage tanks, ensuring that stress distributions and load transfer are accurately represented, which is crucial for the structural integrity of the vessel under operational conditions. The model is an extension of previous research by the authors and existing literature. It has been shown that this model is necessary, in contrast to flat plate models, as it accounts for the coupling between in-plane and out-of-plane behavior and the resulting effects on the stress states.

A limited set of boundary conditions is available to solve the system of unknown scaling coefficients in the solutions to the partial differential equations. Although certain assumptions reduce the number of scaling coefficients, sufficient boundary conditions are not always present, particularly in the case of real or mixed out-of-plane roots. The model accommodates both distinct and repeated in-plane roots, as well as complex out-of-plane roots. However, it lacks sufficient boundary conditions for mixed or all-real out-of-plane roots. It has been demonstrated that the distribution of the roots depends on the design and loading conditions of the vessel. Additional boundary conditions have been proposed, including the rotation of the loading edge, out-of-plane work, and the displacement at the rotationally symmetric edges. Potential benefits and challenges of these boundary conditions have been discussed, such as the interaction between stress fields and the inclusion of pressure loads, which complicate the analysis.

The model has been verified by comparing the results to those obtained from a numerical model created in Abaqus. Discrepancies in stress decay along the vessel length were observed, although it remains unclear whether these are due to errors in the analytical model or the numerical model. Potential improvements to the analytical model and sources of error in the numerical model, such as the rotation of the loading edge or inaccuracies in capturing stress discontinuities, have been identified. Both models will be further refined to bring the results closer together.

Despite the limitations, the model has demonstrated its value in performing preliminary analyses. It has been shown

how the model can be used to study the influence of laminate choice on the decay of concentrated stresses; where 0 layer promote a fast decay in stress, whereas 45 layers yield a more gradual behavior. Additionally, it has been highlighted that cylinder-specific models are required, as different transverse stress behavior is observed compared to flat plate models.

The model contributes to the development of hydrogen storage vessels. In future work, thermal and pressure loads will be incorporated into the loading conditions. This will enable the analysis of how the connectors of a double-walled all-composite hydrogen storage vessel affect the stress state of the composite structure. The model will also be useful in studying the vessel under traditional loading conditions, such as static loads, sloshing, and crash loading, as well as analyzing the potential for the storage vessel to act as a primary structure, where additional loads may be introduced. Ultimately, this work aims to support the aviation industry in its transition toward more sustainable practices.

References

[1] Poorte, V. K., van Campen, J. M. J. F., Bergsma, O. K., and Alderliesten, R. C., "Structural integration of a full-composite, double-walled, vacuum-insulated, cryo-compressed tank for the Flying V: a numerical study," *AIAA SCITECH 2024 Forum*, 2024. https://doi.org/10.2514/6.2024-0834.

[2] Poorte, V. K., Bergsma, O. K., van Campen, J. M. J. F., and Alderliesten, R. C., "Advancing Hydrogen Storage In Aviation: Analysing Load Introduction In All-composite Double-walled Vacuum-insulated Cryo-compressed Vessels," *Proceedings of the 21st European Conference on Composite Materials*, Vol. 8 - Special Sessions, 2024, pp. 605–612.

[3] Kassapoglou, C., *Design and analysis of composite structures: With applications to aerospace structures*, John Wiley Sons, United States, 2010.

[4] Nebe, M., Soriano, A., Braun, C., Middendorf, P., and Walther, F., "Analysis on the mechanical response of composite pressure vessels during internal pressure loading: FE modeling and experimental correlation," *Composites Part B: Engineering*, Vol. 212, 2021, p. 108550. https://doi.org/10.1016/j.compositesb.2020.108550.